Spectra of Ni- and Co-like ions of Xe in an electron-beam ion trap

E. Träbert, P. Beiersdorfer, and M.F. Gu

Abstract: High-resolution soft X-ray observations of Ni- and Co-like Xe ions in an electron-beam ion trap are compared with the predictions of various calculations. Calculated energy levels up to the $4p$ levels are presented alongside experimental determinations.

PACS Nos.: 32.30.Rj; 34.50.Fa; 34.80.Dp

Résumé : Nous comparons avec les prédictions de divers calculs théoriques, les résultats expérimentaux de haute précision des rayons-X mous d'ions Xe de type Ni et Co dans un piège ionique à faisceau d'électrons. Les résultats des calculs de niveaux d'énergie jusqu'aux niveaux $4p$ sont présentés en parallèle avec les données expérimentales.

[Traduit par la Rédaction]

1. Introduction

Nickel-like ions (28 electrons, closed $3d^{10}$ shell ground configuration) are of interest in several areas of physics. One usage of Ni-like ions is in the generation of EUV laser light, exploiting the relative longevity of $3d^9$4d levels that cannot decay directly to the ground state (because of the same parity) by electric dipole (E1) transitions. They decay towards $3d^9\,4p$ levels instead, which in turn rapidly empty towards the ground state. EUV laser physics [1] obviously requires accurate level positions of these levels to optimize the optical elements of EUV lasers. Line coincidences in particular, with transitions in other ions of the same element, in inadvertent impurity ions or in ions of elements deliberately admixed can have either beneficial or deleterious effects on lasing. The reasons are that such coincidences can photo-pump a given transition in the nickel-like ion and thus either enhance the process by adding to the population of the upper level or spoil it by enhancing the population of the lower laser level [2–6]. There are also observations of Ni-like spectra from foil-excited ion beams [7], tokamaks [8–10], laser-produced plasmas [11, 12], and a capillary discharge [13]. The tokamak observations show strong electric quadrupole (E2) transitions that have been modelled for plasma diagnostics based on Co- and Ni-like ions [14]. Observations of Ni-like W ($Z = 74$) and Au ($Z = 79$) ions have been reported from the Livermore electron-beam ion trap [15, 16] in the context of the determination of charge state distributions. In those two studies, the $3d$–$4f$ transitions were partly resolved by means of an X-ray crystal spectrometer, but the $3d$–$4s$ and $3d$–$4p$ transitions were studied by a microcalorimeter yielding spectra of somewhat lower resolution, and the groups of lines therefore appeared like bands. Ralchenko et al. report soft X-ray spectra of Ni-like W ions from microcalorimeter observations of the NIST electron beam ion trap and discuss the use of forbidden transitions in density diagnostics [17, 18]. Ni-like spectra of high-Z ions also play a role in the diagnostics of inertial confinement fusion (ICF) plasmas, Z-pinch plasmas, and ionization balance measurements [19–22]. Very recently, the appearance of bright EUV light emission from the interaction of an intense laser pulse with Xe clusters has been interpreted as relating to Ni-like Xe ions [23].

Theory has tried to provide the required information on Co- and Ni-like ions. However, most of the calculations are incomplete for different reasons, mainly because of the sheer amount of information associated with nickel-like spectra and the lack of precise spectroscopic information to guide the way. For example, Churilov et al. [12] have systematized their laser-produced plasma data for Ni- and Zn-like ions of elements up to $Z = 50$ and compared them with their own calculations. Biémont [24] has calculated various Ni-like ions but only samples at wide intervals of nuclear charge, and Xe is not among them. Quinet and Biémont [25] have studied levels and decay rates of Ni-like ions from Ag XX ($Z = 47$) through Pb LV ($Z = 82$), but they did not include the magnetic octupole decay of the lowest excited level, $3d^9\,4s^3\mathrm{D}_3$ (for a level scheme of the lowest levels, see Fig. 1). Zhang et al. [26] have made calculations from $Z = 60$ upwards. Safronova et al. [27] and Hamasha et al. [28] covered E1 decays only, but neither the E2 nor the M3 decays of the $3d^9\,4s$ levels were included. Badnell et al. [29] performed extensive R-matrix calculations of the excitation and ionization of Ni-like Xe ($Z = 54$), but they explicitly disregarded the M3 decay of the $3d^9\,4s\,3\mathrm{D}_3$ level. Zhong et al. [30] calculated lines for an X-ray laser, but only for Ta ($Z = 73$). Ralchenko et al. [17, 18] have modeled the soft

Received 23 June 2007. Accepted 25 October 2007. Published on the NRC Research Press Web site at http://cjp.nrc.ca/ on 28 March 2008.

E. Träbert,[1,2] P. Beiersdorfer, and M.F. Gu. High Temperature and Plasma Physics Division, Lawrence Livermore National Laboratory, Livermore, CA 94550-9234, USA.

[1]Also at Fakultät für Physik und Astronomie, Ruhr-Universität Bochum, D-44780 Bochum, Germany.
[2]Corresponding author (e-mail: traebert@ep3.ruhr-uni-bochum.de).

 doi: 10.1139/P07-180

Fig. 1. Level scheme of the $3d^{10}$, $3d^9\,4s$, and $3d^9\,4p$ levels of Xe XXVII (Ni-like).

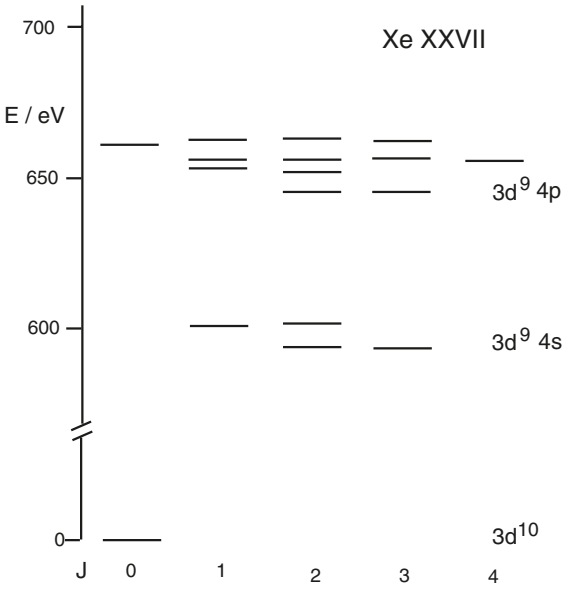

X-ray spectra of Cu- and Ni-like W ions, finding good agreement of synthetic and observed electron-beam ion trap spectra. All ground-state transitions have been treated by Safronova et al. [31] including those in xenon, but information on competing decay paths of the $4s$ levels, which are particularly relevant for the dominant decay branch of the $^3D_1$ level to $^3D_2$, have not yet been addressed. Specific excitation processes have been addressed in calculations of Ni-like ions of Ta ($Z = 73$) and W ($Z = 74$) [32, 33]. No calculations were found that covered all $4s$ and $4p$ levels of Xe XXVII or Xe XXVIII.

The M3 transition rate of the $3d^9\,4s\,^3D_3$ level to the ground state [34, 35] was the focus of a paper by Yao et al. [36], concentrating on Xe and discussing the role of hyperfine quenching in the lifetime of the $3d^9\,4s\,^3D_3$ level. In even isotopes (without hyperfine structure), this level has an exceptionally long lifetime, measured at the Livermore SuperEBIT electron-beam ion trap to be 15.12 ± 0.26 ms [35], in agreement with the prediction by Yao et al. Other calculations differ from this by up to approximately 20%. The long lifetime is of special interest because it differs so much from the other levels in the same configuration, which are predicted to be in the nanosecond and microsecond ranges. The M3 radiative rate is comparable to collision rates in low-density plasmas, and therefore the M3 decay provides a possible density diagnostic tool.[3] Moreover, it has been demonstrated that this specific level plays a role in the delayed response of the charge state distribution in a plasma to sudden changes of external parameters, as well as in the ionization of Ni-like ions at much lower energies than the ionization potential.[3] The charge state then reached is Co-like. In fact, the SuperEBIT soft X-ray spectra of Xe that we describe in this paper are dominated by lines of Ni- and Co-like ions, and we detail the $4s$ and $4p$ level structure of both ions as obtained from the measurements.

[3] E. Träbert, G.V. Brown, M.F. Gu, and S.B. Hansen. Manuscript in preparation.

2. Experiment

The experiment was performed at the electron-beam ion trap (EBIT) laboratory of the University of California at Lawrence Livermore National Laboratory. In an EBIT [37], a high-density electron beam proceeds in ultrahigh vacuum, guided by a magnetic field of a few tesla. The electron beam passes along the symmetry axis of three drift tubes (at different electric potentials) that act as a Penning trap, and with the combination of magnetic field and drift tube voltages ions produced from atoms in the residual gas are trapped. They are bombarded with electrons over and over again, and in the balance of ionization and recombination processes they can be ionized further until the electron beam energy can no longer surpass the ionization potential. The electron beam is almost monoenergetic, with an energy spread of less than 50 eV.

The gas injection in the EBIT system used a ballistic injector with a reservoir pressure of 5×10^{-9} to 3×10^{-6} Torr (1 Torr $\approx$ 133 Pa). The actual pressure in the gas plume upon interaction with the electron beam is estimated to be lower by two orders of magnitude, whereas the background pressure in the EBIT vessel is better than 10^{-11} Torr. With Xe, the injection pressure was in the lower part of the above range. To counter the burning out of the low-Z gas spectra for some of the calibration spectra, pressures in the higher range were used. We obtained time-integrated soft X-ray spectra by using a grazing-incidence flat-field spectrograph [38] with a cryogenic CCD camera as the detector. The spectrograph is based on a variable line spacing grating with a groove density of about 2400 ℓ/mm and a grating radius of curvature of 44.3 m that is used at 2° grazing angle. The emission zone in the EBIT, basically the volume of the exciting electron beam with a diameter of 70 μm [39], was imaged onto the 1340×1300 pixels, each 20 μm square. The typical line width was 2 to 3 pixels, corresponding to a resolving power of about 800 at a wavelength of about 20 Å. The emission zone is somewhat wider for ions in long-lived excited states [40], because they can gyrate out of the excitation zone before emitting radiation; the associated line broadening would need to be taken into account in a detailed study of relative line intensities.

The spectra were calibrated by injecting light gases (CO_2, N_2) into SuperEBIT, providing the well-known resonance lines of H- and He-like ions of C, N, and O [41–43]. The wavelengths of these lines are known from theory and accurate experiments to better than 1 mÅ. The calibration light source is excited by the very same electron beam, and thus it is the very same location as the Xe light source of the production runs. In some of the Xe spectra, $1s$–$2p$ transitions of H- and He-like oxygen appear (O VIII Ly$_\alpha$ at 656 eV, O VII "w" at 560 eV) and provide internal calibration references (Fig. 2). Nevertheless, there is some statistical scatter among the measurements. We have estimated our measurement error from this scatter of a few dozen individual spectra.

The EBIT was run in a cyclic mode, using electron-beam energies of 1.4 keV (producing mostly Ni-like spectra, staying below the ionization potential of 1.5 keV (Fig. 2)) and 1.9 keV (for a stronger production of Co-like spectra (Fig. 3*c*)). The electron beam was switched on for about 30 s, of which the breeding of ions up to the desired charge state required less than

Fig. 2. Xe spectrum (wavelength scale) with calibration lines of oxygen and prominent $3d^9\,4s$ level decays in Xe XXVII indicated. The spectrum was recorded at an electron-beam energy below the ionization limit of the Ni-like ion of Xe. However, except for the calibration lines, the spectrum consists exclusively of lines of Xe XXVII and Xe XXVIII.

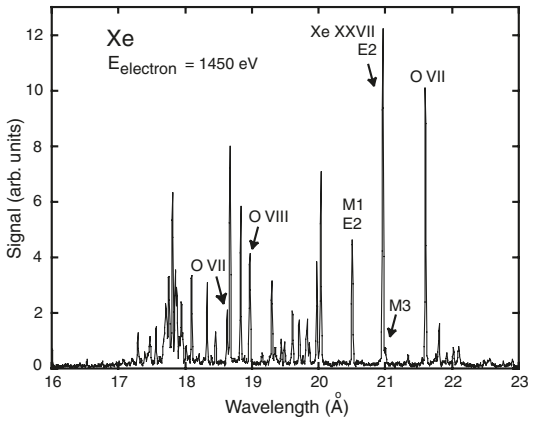

Fig. 3. Synthetic spectrum of (*a*) Xe XXVII (Ni-like) and (*b*) Xe XXVIII (Co-like) from a collisional-radiative model. Spectrum (*c*) is a measurement at an electron-beam energy of 1.9 keV. At this setting, the Xe XXVIII lines are slightly stronger than the Xe XXVII lines. The line groups are easily separated.

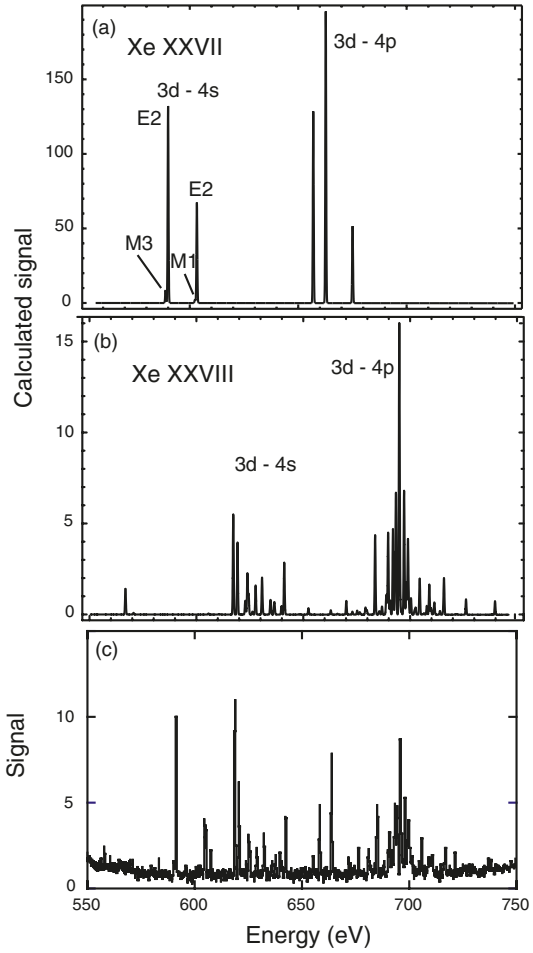

30 ms. At these electron-beam energies, oxygen (as a contaminant leftover from calibrations with CO_2) can be fully ionized, and therefore cycle times of less than 1 s were used in the calibration runs. At the end of each breeding period, the ion cloud was ejected to prevent the build-up of heavy element contaminants, and a new trapping cycle started. Typical exposure times for individual spectra were 20 min, so that the number and density of cosmic ray events on the CCD chip (which would spoil the spectroscopic evaluation) remained manageable.

Table 1 lists the observed lines along with the calibration references. The wavelength uncertainty of 1 to 2 mÅ (depending on counting statistics, proximity of calibration lines, absence of spectral blends) corresponds to an energy uncertainty of 30 to 60 meV. The Xe measurements used natural Xe with several isotopes. The spectral resolution was not high enough to see effects of hyperfine splitting in the isotopes ^{129}Xe and ^{131}Xe that together make up 49% of the natural isotope abundance.

3. Calculations and synthetic spectra

As mentioned in the Introduction, no calculations were found in the literature that covered all of the $4s$ and $4p$ levels of either Xe XXVII or Xe XXVIII. Hence, we used the flexible atomic code (FAC) [44] to provide a systematic basis for the 17 $3d^{10}$, $3d^9\,4s$, and $3d^9\,4p$ levels of Xe XXVII and for the 63 $3d^9$, $3d^8\,4s$, and $3d^8\,4p$ levels of Xe XXVIII. The $4d$ levels of each spectrum were included in the calculations, but with the exception of a few transitions mediated by configuration interaction (two-electron transitions), the decays of these levels fall outside the range of our experimental observations.

FAC is not set up to produce extremely accurate level values, but it is easy to set up and run and it can handle a vast number of levels and transitions as needed for collisional-radiative modeling. For the present project, the model assumptions were an electron-beam energy of 2.5 keV and an electron density of 10^{11} cm^{-3}. The assumed electron-beam energy is higher than the one actually used, but this difference has been found to be of secondary importance in other applications. The calculations resulted in energy levels (Tables 2 and 3) and in lists of spectral lines with transition energies and relative intensities. To compare the computed spectra with the measured ones, the calculated spectra were convoluted with a Gaussian line shape of 0.5 eV FWHM. The resulting synthetic spectra are strikingly similar to the observed ones (Fig. 3). It is straightforward to identify isolated lines from the calculations, and we do so in Table 1 and correspondingly add experimental energies for comparison to the levels presented in Tables 2 and 3. However, the calculations also yield a large number of individually weak lines, some of which cluster and make up what appear to be individual lines. The numerous blends among the Xe XXVIII $3d$–$4p$ lines make it difficult to compare individual transition energies with the measured line positions, and we elect to identify the blending transitions in Table 1 but without listing the calculated transition energies of the contributors. Those can be established from the term values given in Table 2.

The pattern of predicted relative line intensities is easily reconciled with observation within each group of lines. The relative intensities of $4s$ versus $4p$ level decays differ between calculation and observation because the detection efficiency (including

Table 1. Line list from observation.

		Experiment			Theory Xe XXVII		Xe XXVII upper level
Identification spectrum	Ref. lambda (Å)	Lambda (Å)	Signal	Energy (eV)	Lambda (Å)	Energy (eV)	Xe XXVIII transition
O VIII 1-3	16.006[a]	16.007	6.5	774.58			
Xe XXVIII		17.294	14.0	716.92			0–57, 0–58
O VII 1-5	17.396[b]	17.401	5.2	712.51			
Xe XXVIII		17.472	15.0	709.62			1–62
Xe XXVIII		17.563	18.0	705.94			0–46
Xe XXVIII		17.713	44.6	699.96			0–39, 1–54
O VII 1-4	17.768[b]	17.756 bl	60.4	698.27			
Xe XXVIII		bl					0–38, 1–52
Xe XXVIII		17.811	116.	696.11			0–37, 1–49
Xe XXVIII		17.853	63.0	694.47			0–34, 0–35, 1–47
Xe XXVIII		17.878	46.0	693.50			0–33
Xe XXVIII		17.920	16.0	691.88			1–45
Xe XXVIII		17.949	38.0	690.76			0–28, 1–42, 1–29
Xe XXVIII		18.096	48.0	685.15			0–21, 0–25
Unknown		18.202	4.0	681.16			
Xe XXVII		18.328 bl	38.0	676.47	18.338[c]	676.11	$3d4p\ ^1P_1$
		18.326[d]			18.365	675.11[e]	15
Xe XXVIII		bl					1–28
Unknown		18.456	14.0	671.78			
O VII 1-3	18.6284[b]	18.630	27.7	665.53			
Xe XXVII		18.675	147	663.92	18.686[c]	663.51	$3d4p\ ^3D_1$
		18.667[d]			18.708	662.72[e]	11
Xe XXVIII		bl					1–23
Xe XXVII		18.833	92.0	658.34	18.846[c]	657.88	$3d4p\ ^3P_1$
		18.826[d]			18.872	656.97[e]	8
O VIII 1-2	18.968[a]	18.970	69.0	653.58			
Xe XXVIII		bl					1–20
Unknown		19.153	5.0	647.34			
Xe XXVIII		19.300	45.0	642.41			0–15
Unknown		19.350	9.3	640.75			
Xe XXVIII		19.442	12.8	637.71			0–12
Xe XXVIII		19.492	9.3	636.08			1–18, 1–19
Xe XXVIII		19.609	30.0	632.28			0–9, 0–10
Xe XXVIII		19.711	25.8	629.01			1–16
Xe XXVIII		19.827	31.0	625.33			0–7, 0–8
Xe XXVIII		19.862	11.0	624.23			1–12
Xe XXVIII		19.974	63.5	620.73	20.021	619.26[e]	0–6
Xe XXVIII		20.034	135	618.87	20.087	617.25[e]	0–5, 1–10
Xe XXVII E2		20.506	81.7	604.62	20.518[c]	604.27	$3d4s\ ^1D_2$
		20.502[d]			20.552	603.27[e]	4
Xe XXVII M1					20.549[c]	603.36	$3d4s\ ^3D_1$
					20.582	602.40[e]	3
Xe XXVII E2		20.964	250	591.42	20.978[c]	591.02	$3d4s\ ^3D_2$
		20.961[d]			21.014	590.00[e]	2
Xe XXVII M3		21.003	8.5	590.32	21.015[c]	589.98	$3d4s\ ^3D_3$
					21.056	588.84[e]	1
Unknown		21.344	4.2	580.89			
O VII "w"	21.6015[f]	21.603	205	573.93			
Unknown		21.765	6.2	569.65			
O VII "y"	21.8036[f]	21.804	24.2	568.63			
Unknown		21.924	5.1	565.52			

Table 1. (*concluded*).

Identification spectrum	Ref. lambda (Å)	Experiment			Theory Xe XXVII		Xe XXVII upper level
		Lambda (Å)	Signal	Energy (eV)	Lambda (Å)	Energy (eV)	Xe XXVIII transition
Unknown		22.021	8.1	563.03			
O VII "z"	22.0977[f]	22.099	10.6	561.04			
Unknown		22.581	4.5	549.06			

Note: The oxygen reference lines and their positions as determined from the calibration are included to show the uncertainty of the calibration scale, which is of the order of 2 mÅ. The energy values have been rounded to reflect the experimental uncertainty. Safronova et al. [31] provide wavelengths and LS level notation for Ni-like ions, and we give our calculational results on Xe XXVII for comparison, as well as conversions into energy and vice versa. The energies and upper level numbers from our own calculations (two right-most columns) refer to Tables 2 (Ni-like ion) and 3 (Co-like ion), respectively. Our collisional-radiative model yielded relative line intensities (see Fig. 2) that are in good qualitative agreement with the observed relative intensities in column 4.
[a]Ref. 41
[b]Ref. 43
[c]Ref. 42
[d]Ref. 31
[e]FAC calculation, this work
[f]Ref. 8

Table 2. $4s$ and $4p$ levels of Xe XXVII (Ni-like ion).

Index	Theory (this work)		LS-coupling label	Other theory [31]	Experiment
	Energy (eV)	jj-Coupling identifier		Energy (eV)	Energy (eV)
$3d^{10}$					
0	0	$3d^6_{5/2}(J=0)$			
$3d^9\,4s$					
1	588.84	$3d^5_{5/2}\,4s_{1/2}(J=3)$	^{3}D$_3$	589.98	590.32
2	590.00	$3d^5_{5/2}\,4s_{1/2}(J=2)$	^{3}D$_2$	591.02	591.42
3	602.40	$3d^3_{3/2}\,4s_{1/2}(J=1)$	^{3}D$_1$	603.36	
4	603.27	$3d^3_{3/2}\,4s_{1/2}(J=2)$	^{1}D$_2$	604.27	604.62
$3d^9\,4p$					
5	641.57	$3d^5_{5/2}\,4p_{1/2}(J=2)$	^{3}F$_2$	642.61	
6	642.61	$3d^5_{5/2}\,4p_{1/2}(J=3)$	^{3}F$_3$	643.67	
7	655.36	$3d^3_{3/2}\,4p_{1/2}(J=2)$	^{3}P$_2$	656.38	
8	656.97	$3d^3_{3/2}\,4p_{1/2}(J=1)$	^{3}P$_1$	657.88	658.34
9	660.38	$3d^5_{5/2}\,4p_{3/2}(J=4)$	^{3}F$_4$		
10	661.96	$3d^5_{5/2}\,4p_{3/2}(J=2)$	^{1}D$_2$	663.02	
11	662.72	$3d^5_{5/2}\,4p_{3/2}(J=1)$	^{3}D$_1$	663.51	663.92
12	663.57	$3d^5_{5/2}\,4p_{3/2}(J=3)$	^{1}F$_3$	664.55	
13	671.72	$3d^3_{3/2}\,4p_{3/2}(J=0)$	^{3}P$_0$		
14	674.92	$3d^3_{3/2}\,4p_{3/2}(J=3)$	^{3}D$_3$	675.96	
15	675.11	$3d^3_{3/2}\,4p_{3/2}(J=1)$	^{1}P$_1$	676.11	676.47
16	676.64	$3d^3_{3/2}\,4p_{3/2}(J=2)$	^{3}D$_2$	677.55	

Note: The calculated energy values have been rounded to 10 meV. The experimental energies are uncertain by 30 to 50 meV.

the polarization response) of the spectrograph and its dependence on wavelength have not been established, and therefore the observations have not been corrected for this technical effect. However, no drastic variation is expected across the range of the present spectra. Of course, the population model implied in the collisonal-radiative model calculations has not been calibrated either.

4. Term analysis

Atomic levels in multiply charged ions of elements in the middle of the table of the elements would in most cases be appropriately described in intermediate coupling, which is somewhat cumbersome. Following the labeling choices made by Safronova et al. [31] for the Xe XXVII $4p$ levels (which we have completed in Table 2), one finds irregular level sequences

Table 3. Levels of Xe XXVIII (Co-like ion).

	Theory (This work)		Experiment
Index	Level energy (eV)	jj-Coupling identifier	Energy (eV)
$3s^2\,3p^6\,3d^9$			
0	0.0	$3d^5_{5/2}(J=5/2)$	
1	13.581	$3d^3_{3/2}(J=3/2)$	
$3s^2\,3p^5\,3d^{10}$			
2	258.17	$3p^3_{3/2}(J=3/2)$	
3	323.56	$3p_{1/2}(J=1/2)$	
$3^1\,3p^6\,3d^{10}$			
4	466.09	$3s_{1/2}(J=12)$	
$3s^2\,3p^6\,3d^8\,4s$			
5	617.25	$3d^4_{5/2}\,4s_{1/2}(J=9/2)$	618.87 E2
6	619.26	$3d^4_{5/2}\,4s_{1/2}(J=7/2)$	620.73 M1/E2
7	623.89	$3d^4_{5/2}\,4s_{1/2}(J=5/2)$	624.23 bl M1/E2
8	624.46	$3d^4_{5/2}\,4s_{1/2}(J=3/2)$	625.33 bl M1
9	630.72	$3d^3_{3/2}\,3d^5_{5/2}4s_{1/2}(J=7/2)$	632.28 bl
10	631.01	$3d^3_{3/2}\,3d^5_{5/2}4s_{1/2}(J=5/2)$	632.28 bl
11	634.59	$3d^4_{5/2}\,4s_{1/2}(J=1/2)$	636.08
12	636.44	$3d^3_{3/2}\,3d^5_{5/2}4s_{1/2}(J=5/2)$	637.71 bl
13	636.69	$3d^3_{3/2}\,3d^5_{5/2}4s_{1/2}(J=3/2)$	637.71 bl
14	639.82	$3d^3_{3/2}\,3d^5_{5/2}4s_{1/2}(J=3/2)$	640.75
15	641.12	$3d^3_{3/2}\,3d^5_{5/2}4s_{1/2}(J=9/2)$	642.41 bl
16	641.30	$3d^3_{3/2}\,3d^5_{5/2}4s_{1/2}(J=7/2)$	642.41 bl
17	641.38	$3d^3_{3/2}\,3d^5_{5/2}4s_{1/2}(J=1/2)$	642.41 bl
18	648.18	$3d^2_{3/2}\,4s_{1/2}(J=3/2)$	
19	648.43	$3d^2_{3/2}\,4s_{1/2}(J=5/2)$	
20	666.02	$3d^2_{3/2}\,4s_{1/2}(J=1/2)$	
$3s^2\,3p^6\,3d^8\,4p$			
21	670.16	$3d^4_{5/2}\,4p_{1/2}(J=7/2)$	671.78
22	671.52	$3d^4_{5/2}\,4p_{1/2}(J=9/2)$	
23	676.47	$3d^4_{5/2}\,4p_{1/2}(J=3/2)$	
24	676.90	$3d^4_{5/2}\,4p_{1/2}(J=5/2)$	
25	683.62	$3d^3_{3/2}\,3d^5_{5/2}\,4p_{1/2}(J=5/2)$	685.15 bl
26	683.71	$3d^3_{3/2}\,3d^5_{5/2}\,4p_{1/2}(J=7/2)$	685.15 bl
27	686.58	$3d^4_{5/2}\,4p_{1/2}(J=1/2)$	
28	688.84	$3d^3_{3/2}\,3d^5_{5/2}\,4p_{1/2}(J=3/2)$	690.76
29	689.77	$3d^3_{3/2}\,3d^5_{5/2}\,4p_{1/2}(J=5/2)$	
30	690.07	$3d^4_{5/2}\,4p_{3/2}(J=11/2)$	
31	691.45	$3d^3_{3/2}\,3d^5_{5/2}\,4p_{1/2}(J=1/2)$	
32	691.77	$3d^4_{5/2}\,4p_{3/2}(J=9/2)$	
33	692.00	$3d^4_{5/2}\,4p_{3/2}(J=7/2)$	693.50
34	693.28	$3d^3_{3/2}\,3d^5_{5/2}\,4p_{1/2}(J=3/2)$	694.47 bl
35	693.43	$3d^4_{5/2}\,4p_{3/2}(J=5/2)$	694.47 bl
36	694.02	$3d^3_{3/2}\,3d^5_{5/2}\,4p_{1/2}(J=9/2)$	
37	694.96	$3d^3_{3/2}\,3d^5_{5/2}\,4p_{1/2}(J=7/2)$	696.11
38	697.18	$3d^4_{5/2}\,4p_{3/2}(J=5/2)$	689.27

Table 3. (*concluded*.)

	Theory (This work)		Experiment
Index	Level energy (eV)	jj-Coupling identifier	Energy (eV)
$3s^2\,3p^6\,3d^8\,4p$			
39	698.24	$3d^4_{5/2}\,4p_{3/2}(J=7/2)$	699.96
40	699.00	$3d^4_{5/2}\,4p_{3/2}(J=3/2)$	
41	699.35	$3d^4_{5/2}\,4p_{3/2}(J=1/2)$	
42	700.45	$3d^2_{3/2}\,4p_{1/2}(J=5/2)$	
43	702.58	$3d^2_{3/2}\,4p_{1/2}(J=3/2)$	
44	703.41	$3d^3_{3/2}\,3d^5_{5/2}\,4p_{3/2}(J=9/2)$	
45	704.21	$3d^3_{3/2}\,3d^5_{5/2}\,4p_{3/2}(J=5/2)$	705.94 bl
46	704.51	$3d^3_{3/2}\,3d^5_{5/2}\,4p_{3/2}(J=7/2)$	705.94 bl
47	706.50	$3d^3_{3/2}\,3d^5_{5/2}\,4p_{3/2}(J=3/2)$	
48	709.00	$3d^4_{5/2}\,4p_{3/2}(J=3/2)$	
49	709.03	$3d^3_{3/2}\,3d^5_{5/2}\,4p_{3/2}(J=5/2)$	
50	709.60	$3d^3_{3/2}\,3d^5_{5/2}\,4p_{3/2}(J=1/2)$	
51	709.80	$3d^3_{3/2}\,3d^5_{5/2}\,4p_{3/2}(J=7/2)$	
52	710.98	$3d^3_{3/2}\,3d^5_{5/2}\,4p_{3/2}(J=3/2)$	
53	712.77	$3d^3_{3/2}\,3d^5_{5/2}\,4p_{3/2}(J=11/2)$	
54	712.98	$3d^3_{3/2}\,3d^5_{5/2}\,4p_{3/2}(J=5/2)$	
55	713.71	$3d^3_{3/2}\,3d^5_{5/2}\,4p_{3/2}(J=1/2)$	
56	714.00	$3d^3_{3/2}\,3d^5_{5/2}\,4p_{3/2}(J=5/2)$	
57	715.60	$3d^3_{3/2}\,3d^5_{5/2}\,4p_{3/2}(J=3/2)$	716.92
58	715.88	$3d^3_{3/2}\,3d^5_{5/2}\,4p_{3/2}(J=7/2)$	
59	717.16	$3d^3_{3/2}\,3d^5_{5/2}\,4p_{3/2}(J=9/2)$	
60	719.32	$3d^2_{3/2}\,4p_{1/2}(J=1/2)$	
61	720.49	$3d^2_{3/2}\,4p_{3/2}(J=3/2)$	
62	721.42	$3d^2_{3/2}\,4p_{3/2}(J=5/2)$	
63	721.88	$3d^2_{3/2}\,4p_{3/2}(J=7/2)$	
64	724.66	$3d^2_{3/2}\,4p_{3/2}(J=1/2)$	
65	739.76	$3d^2_{3/2}\,4p_{3/2}(J=3/2)$	

Note: The calculated energies have been rounded to 10 meV. bl indicates a line blend.

in the level multiplets. Without an analysis of the level structure along the isoelectronic sequence (for which there is a shortage of experimental data), labeling by first principles is a fruitless exercise. Theory can indicate the major components contributing to a given level, but there is no actual need for the presentation of level labels in a given notation. Anyway, the level density of the $4p$ configuration makes it difficult to discern LS-coupling level multiplets, and we elect to present the jj-coupling notation as used in FAC.

Comparing the Xe XXVII results of our FAC calculations with those of a many-body perturbation theory (MBPT) calculation by Safronova et al. [31] and with experiment, we note that the MBPT level values are about 0.4 eV lower than the measured ones, and the FAC results are about another 1 eV lower. A similar deviation between experiment and FAC results apparently holds for the Xe XXVIII levels (see Table 3), but the actual differences between observed and measured $4s$ and $4p$ level energies range from 0.8 to 1.8 eV. Transitions between the $3d^9$ ground configuration and the $3d^8\,4s$ levels can be M1 or E2 (both are of even parity) transitions, as far as the J values can match the required arithmetic. These M1 and E2 transitions are a hallmark of the new Ni- and Co-like spectra, and they point to the high-Z spectra in which these transitions dominate [45]. For the decays of the $3d^8\,4p$ levels, E1 transitions should be dominant, and the $J = 5/2$ and $J = 3/2$ levels of the ground term can connect to $J = 1/2$, 3/2, 5/2, and 7/2, but not to the $J = 9/2$ and 11/2 levels. Most of the expected decays are, in fact, seen, although some of them are blended. With very few exceptions, all lines in the spectrum recorded can be identified with Xe XXVII, Xe XXVIII, or with calibration lines of O VII and O VIII.

5. Summary of results

Our soft X-ray spectra of Xe are the best-resolved yet in the range from 570 to 730 eV. The earlier data on Xe XXVII as reported by Wyart et al. [8] agree with our measurements well within their larger uncertainties. Our data on Co- and Ni-like ions of Xe add to the range of nuclear charges that were covered in earlier studies that used laser-produced plasmas. The now enlargened and improved data set should be useful for future systematizations towards even higher nuclear charges.

Assisted by FAC calculations, we have identified almost all of the lines in our observation range. The results of several calculations (MBPT and FAC) have been compared with the experimental data. The results of the calculations for Xe XXVII differ most by their offset of the ground-state energy (0.4 eV for the MBPT calculations by Safronova et al. [31], 1.4 eV for the present FAC calculations), which can be corrected for in a first step towards semi-empirically adjusted reference values. Considering the scatter of the predicted level energies after such an adjustment, the FAC calculations scatter by as little as about 0.1 to 0.2 eV around the experimental level values for Xe XXVII and about 0.4 eV for Xe XXVIII, just as the results of much more extensive calculations do. For many practical purposes, such as the identification of the more prominent spectral lines by the transition energy and by relative line intensities, the very fast FAC calculations should not only be appropriate for exploratory research but yield results as good as those of more cumbersome atomic codes.

The very recent study of the X-ray spectrum of tungsten [17] purports to report on Ni- and Co-like spectra too. However, the microcalorimeter used has a lower resolving power than our grating spectrometer, and the Co-like ion contribution to the W spectrum appears to be much weaker under the conditions of that experiment. Our observations, supported by our calculations, show that under low-density conditions the E2 transitions in Co-like ions are comparable in intensity to the E2 and M3 transitions in Ni-like ions of Xe. This observation supports the suggestion (made earlier for the E2 lines [14]) that the M3 transitions should be added to the inventory of lines that can be employed for density diagnostics.

Acknowledgement

We are happy to acknowledge the dedicated technical support of Ed Magee and Phil D'Antonio, and help with running the experiment by G.V. Brown, H. Chen, J.T. Clementson, and D.B. Thorn. ET acknowledges travel support by the German Research Association (DFG). The work at the University of California Lawrence Livermore National Laboratory was performed under the auspices of the Department of Energy under Contract No. W-7405-Eng-48.

References

1. J. Nilsen. Phys. Scr. **43**, 596 (1991).
2. P. Beiersdorfer, J. Nilsen, A. Osterheld, D. Vogel, K. Wong, R.E. Marrs, and R. Zasadzinski, Phys. Rev. A, **46**, R25 (1992).
3. S. Elliott, P. Beiersdorfer, and J. Nilsen. Phys. Rev. A, **47**, 1403 (1993).
4. S.R. Elliott. Phys. Scr. **49**, 556 (1994).
5. S.R. Elliott, P. Beiersdorfer, and J. Nilsen. Phys. Rev. A, **51**, 1683 (1995).
6. S.R. Elliott, P. Beiersdorfer, B.J. MacGowan, and J. Nilsen. Phys. Rev. A, **52**, 2689 (1995).
7. C.L. Cocke, S.L. Varghese, J.A. Bednar, C.P. Bhalla, B. Curnutte, R. Kauffman, R. Randall, P. Richard, C. Woods, and J.H. Scofield. Phys. Rev. A, **12**, 2413 (1975).
8. J.-F. Wyart, C. Bauche-Arnoult, and E. Luc-Koenig. Phys. Scr. **32**, 103 (1985).
9. S. von Goeler, P. Beiersdorfer, M. Bitter, R. Bell, K. Hill, P. LaSalle, L. Ratzan, J. Stevens, J. Timberlake, S. Maxon, and J. Scofield. J. Phys. Coll. **40**, C1-181 (1988).
10. K.B. Fournier, W.H. Goldstein, M. May, M. Finkenthal, and J.L. Terry. Phys. Rev. A, **53**, 3110 (1996).
11. J.-F. Wyart, C. Bauche-Arnoult, J.-C. Gauthier, J.-P. Geindre, P. Monier, M. Klapisch, A. Bar-Shalom, and A. Cohn. Phys. Rev. A, **34**, R701 (1986).
12. S.S. Churilov, A.N. Ryabtsev, and J.-F. Wyart. Phys. Scr. **38**, 326 (1988).
13. A. Rahman, J.J. Rocca, and J.F. Wyart. Phys. Scr. **70**, 21 (2004).
14. K.B. Fournier, W.H. Goldstein, M. May, and M. Finkenthal. Phys. Rev. A, **53**, 709 (1996).
15. M.J. May, K.B. Fournier, P. Beiersdorfer, H. Chen, and K.L. Wong. Phys. Rev. E, **68**, 036402 (2003).
16. P. Neill, C. Harris, A.S. Safronova, S. Hamasha, S. Hansen, U.I. Safronova, and P. Beiersdorfer. Can. J. Phys. **82**, 931 (2004).
17. Yu. Ralchenko, J.N. Tan, J.D. Gillaspy, J.M. Pomeroy, and E. Silver. Phys. Rev. A, **74**, 042514 (2006).
18. Yu. Ralchenko. J. Phys. B: At. Mol. Opt. Phys. **40**, F175 (2007).
19. C. Chenais-Popovics, V. Malka, J.-C. Gauthier, S. Gary, O. Peyrusse, M. Rabec-Le Gloahec, I. Matsushima, C. Bauche-Arnoult, A. Bachelier, and J. Bauche. Phys. Rev. A, **65**, 046418 (2002).
20. S.H. Glenzer, K.B. Fournier, B.G. Wilson, R.W. Lee, and L.J. Suter. Phys. Rev. Lett. **87**, 045002 (2001).
21. K.L. Wong, M.J. May, P. Beiersdorfer, K.B. Fournier, B. Wilson, G.V. Brown, P. Springer, P.A. Neill, and C.L. Harris. Phys. Rev. Lett. **90**, 235001 (2003).
22. A. Safronova, V. Kantsyrev, A. Esaulov, D. Fedin, N. Ouart, F. Yilmaz, G. Osborne, V. Nalajala, S. Pokala, I. Shrestha, A. Astanovitsky, S. Batie, B. LeGalloudec, T. Cowan, B. Jones, C. Coverdale, C. Deeney, D. LePell, and J. Gradel. AIP Conf. Proc. **808**, 149 (2006).
23. E.P. Ivanova and A.L. Ivanov. J. Exp. Theor. Phys. **100**, 844 (2005).
24. E. Biémont. J. Phys. B: At. Mol. Opt. Phys. **30**, 4207 (1997).
25. P. Quinet and E. Biémont. Phys. Scr. **43**, 150 (1991).
26. H.L. Zhang, D.H. Sampson, and C.J. Fontes. At. Data Nucl. Data Tables, **48**, 91 (1991).
27. U.I. Safronova, W.R. Johnson, and J.R. Albritton. Phys. Rev. A, **62**, 052505 (2000).
28. S.M. Hamasha, A.S. Shlyaptseva, and U.I. Safronova. Can. J. Phys. **82**, 331 (2004).
29. N.R. Badnell, K.A. Berrington, H.P. Summers, M.G. O'Mullane, A.D. Whiteford, and C.P. Ballance. J. Phys. B: At. Mol. Opt. Phys. **37**, 4589 (2004).

30. J.Y. Zhong, J. Zhang, J.L. Zeng, G. Zhao, and M.F. Gu. At. Data Nucl. Data Tables, **89**, 101 (2005).
31. U.I. Safronova, A.S. Safronova, S.M. Hamasha, and P. Beiersdorfer. At. Data Nucl. Data Tables, **92**, 47 (2006).
32. T.M. Shen, C.Y. Chen, Y.S. Wang, Y.M. Zou, and M.F. Gu. Phys. Rev. E, **76**, 022703 (2007).
33. T.M. Shen, C.Y. Chen, Y.S. Wang, Y.M. Zou, and M.F. Gu. J. Phys. B: At. Mol. Opt. Phys. **40**, 3075 (2007).
34. E. Träbert, P. Beiersdorfer, G.V. Brown, S. Terracol, and U.I. Safronova. Nucl. Instrum. Methods Phys. Res. Sect. B, **235**, 23 (2005).
35. E. Träbert, P. Beiersdorfer, G.V. Brown, K.R. Boyce, R.L. Kelley, C.A. Kilbourne, F.S. Porter, and A. Szymkowiak. Phys. Rev. A, **73**, 022508 (2006).
36. K. Yao, M. Andersson, T. Brage, R. Hutton, P. Jönsson, and Y. Zou. Phys. Rev. Lett. **97**, 183001 (2006); Erratum Phys. Rev. Lett. **98**, 269903 (2007).
37. M.A. Levine, R.E. Marrs, J.N. Bardsley, P. Beiersdorfer, C.L. Bennett, M.H. Chen, T. Cowan, D. Dietrich, J.R. Henderson, D.A. Knapp, A. Osterheld, B.M. Penetrante, M.B. Schneider, and J.H. Scofield. Nucl. Instrum. Methods Phys. Res. Sect. B, **43**, 431 (1989).
38. P. Beiersdorfer, E.W. Magee, E. Träbert, H. Chen, J.K. Lepson, M.-F. Gu, and M. Schmidt. Rev. Sci. Instrum. **75**, 3723 (2004).
39. S.B. Utter, P. Beiersdorfer, J.R. Crespo-LÓpez-Urrutia, and K. Widmann. Nucl. Instrum. Methods Phys. Res. Sect. A, **428**, 276 (1999).
40. E. Träbert, S.B. Utter, and P. Beiersdorfer. Phys. Lett. A, **272**, 86 (2000).
41. J.D. Garcia and J.E. Mack. J. Opt. Soc. Am. **55**, 654 (1965).
42. G.W.F. Drake. Can. J. Phys. **66**, 586 (1988).
43. L. Engström and U. Litzén. J. Phys. B: At. Mol. Opt. Phys. **28**, 2565 (1995).
44. M.F. Gu. Can. J. Phys. **86**, 191 (2008).
45. P. Beiersdorfer, A.L. Osterheld, J. Scofield, B. Wargelin, and R.E. Marrs. Phys. Rev. Lett. **67**, 2272 (1991).